Korean J. Chem. Eng., 39(7), 1659-1672 (2022)
DOI: 10.1007/s11814-021-1021-z

pISSN: 0256-1115
eISSN: 1975-7220

REVIEW PAPER

A non-aqueous phase extraction system using tributyl phosphate for H_3PO_4 separation from wet-process superphosphoric acid: Extraction equilibrium and mechanism

Haozhou Liu, Jingxu Yang, Xiuying Yang, Chao Hu, and Lin Yang†

School of Chemical Engineering, Sichuan University, Research Center for Comprehensive Utilization and Clean Processing Engineering of Phosphorus Resources, Ministry of Education, Chengdu 610065, China
(*Received 28 September 2021 • Revised 9 November 2021 • Accepted 20 November 2021*)

Abstract−Conventional wet-process phosphoric acid (WPA) extraction route encounters unsatisfactory extraction efficiency, phosphorus yield, and raffinate utilization. Herein, a new extraction route for H_3PO_4 separation from wet-process superphosphoric acid (WSPA) is proposed to improve these dilemmas. We focus on the equilibrium of H_3PO_4 extraction by tributyl phosphate (TBP) from WSPA and the extraction mechanism of TBP under high H_3PO_4 loading conditions. Several critical factors affecting the extraction equilibrium were investigated to optimize the extraction process, including the initial phase ratio (R_0), the volume fraction of TBP in extractant (φ_{TBP}), temperature (T), and the crosscurrent extraction stages. The results show that the single-stage extraction rate of H_3PO_4 reaches 70% at R_0=6, φ_{TBP}=80% and T=80 °C with separation factors $\beta_{P/Fe}$, $\beta_{P/Al}$, $\beta_{P/Mg}$, and $\beta_{P/Ca}$ of 12.48, 21.66, 47.57, and 8.89, respectively. In addition, Fourier transform infrared spectroscopy and Raman spectroscopy enlighten the extraction mechanism at high loading conditions. The characteristic peak positions of P=O, P=O···H_2O, and P=O···H_3PO_4 in the infrared spectra are determined to be centered at 1,283, 1,267, and 1,233 cm^{-1}, respectively. The semi-quantitative analysis implies that the self-polymerization behavior of the extraction complex TBP·H_3PO_4 and the mutual attraction of reverse micelles (RMs) through their polar cores is the trigger for the formation of a third phase. Furthermore, the red shift of P-$(OH)_3$ asymmetrical stretching vibration in the Raman spectrum indicates the formation of hydrogen bonds among H_3PO_4 molecules in the organic phase, which corroborates the formation of RMs. Conclusions can be obtained that H_3PO_4 enters the organic phase under high loading capacity by reversed micellar extraction. The feasibility of this extraction process is further tested by scrubbing, stripping, and cycling performance experiments. The results are promising for the design of a new efficient route for separating H_3PO_4 from WPA.

Keywords: Wet-phosphoric Acid, Extraction, TBP, Superphosphoric Acid, Non-aqueous Phase Extraction

INTRODUCTION

Phosphoric acid, one of the bulk products in the inorganic phosphorus chemical industry, is widely used in fertilizers, detergents, pharmaceuticals, electronics, and other industries. The wet process is its primary production route, involving digesting phosphate rocks in a mineral acid and purifying the leachate (the leachate is defined as the wet-process phosphoric acid, WPA). The purification section is crucial in obtaining high purity phosphoric acid. In general, there are two thoughts for the separation of H_3PO_4 from WPA: One is to remove the impurity ions from the WPA and the other is to extract H_3PO_4 molecules directly. Separation methods developed from these two perspectives include chemical precipitation, solvent extraction, ion exchange, membrane separation, and crystallization. Among them, solvent extraction is commonly used in industrial WPA purification for its good selectivity and suitability for large-scale production. However, in conventional industrial purification processes, the unsatisfactory extraction efficiency, phosphorus yield for the whole process, and raffinate utilization has become intractable. In particular, the raffinate, which accounts for approximately 30% of the total phosphorus content in the WPA, is difficult to utilize due to the impurity enrichment and low phosphorus content [1]. A new H_3PO_4 extraction process is urgently needed to avoid these shortcomings.

In the purification of WPA by solvent extraction, the extraction for impurity ions and the extraction for H_3PO_4 molecules have their limitations. With regard to the extraction of impurity ions, researchers have reported a large number of viable separation systems. Examples are the removal of Fe^{3+} [2,3], Al^{3+} [4], Mg^{2+} [5], and Zn^{2+} [6] from WPA. It is characterized by simplicity of operation and low phosphorus losses, but the degree and type of impurity ion removal is limited. The resulting purified acid is not yet up to industrial phosphoric acid standards (*The Chinese National Standard of GB/T 2091-2008* [7]). In fact, qualified industrial phosphoric acid is obtained by direct extraction of H_3PO_4 from WPA. Alcohols [8], ethers [9], ketones [10], phospholipids [11], amines [12], and sulfite extractants [13] are commonly used for the separation of H_3PO_4 molecules in WPA. However, due to the selectivity of these extractants, the process requires high quality feedstock phosphoric acid, which is not compatible with the phosphate rock deficiency and dilution in China [14].

In this work, the idea of separating metallic ions (MI) by extraction followed by an H_3PO_4 extraction process is proposed [15]. The new process route is shown in Fig. 1. First, the organic mat-

†To whom correspondence should be addressed.
E-mail: 18980632893@163.com

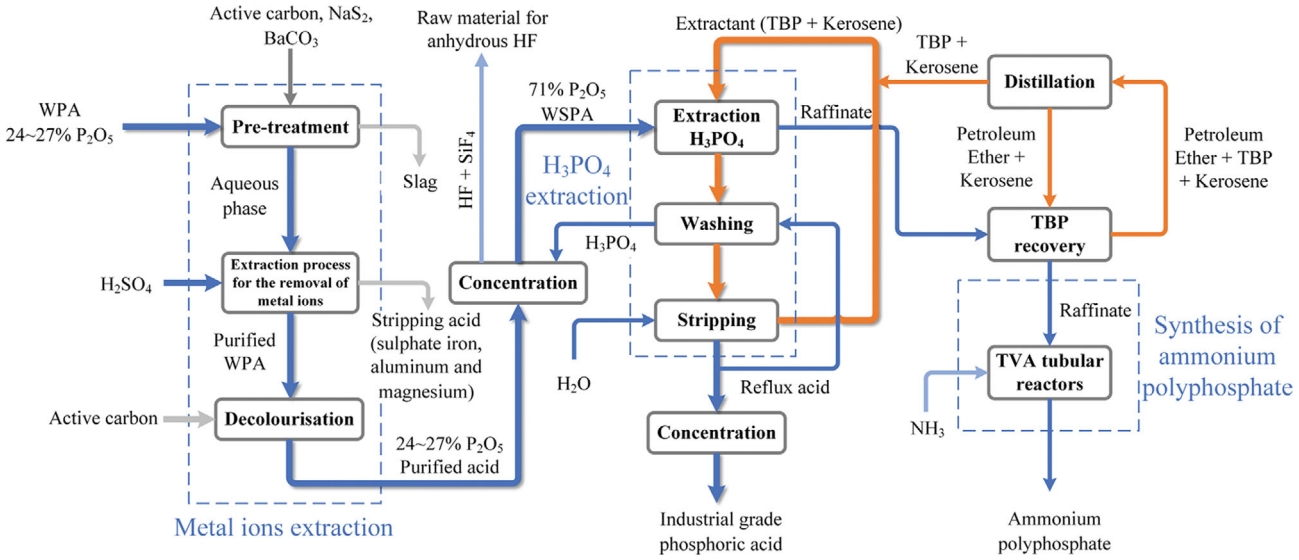

Fig. 1. The wet-process phosphoric acid (WPA) purification route.

Table 1. A comparison between the new process and traditional process for purification of wet-process phosphoric acid by TBP

Items	Previous process	This work
Requirements for raw phosphoric acid	High quality wet-phosphoric acid, MER*=0.04	No restriction
Yield of phosphoric acid product for the whole process	50%	70%
H_3PO_4 loading of extractant	0.15 g P_2O_5/mL extractant	0.17 g P_2O_5/mL extractant
Extraction operating conditions	O/A=4, Four-stage countercurrent extraction, T=50 °C	O/A=6, Single-stage extraction, T=80 °C
Extraction rate determination steps	Mixed-control-model for interfacial reaction and aqueous phase diffusion	Interfacial reaction
By-products	Low value slag acid from concentration	Sulphate crystals of iron, aluminum and magnesium
Utilization of raffinate	Mixing of raffinate with wet-phosphoric acid and ammonification to produce monoammonium phosphate (MAP)	Raffinate is used to produce ammonium polyphosphate (APP) by the TVA process

MER*: An evaluation index of impurity content in phosphoric acid solution, MER=$(w_{Fe_2O_3}+w_{Al_2O_3}+w_{MgO})/w_{P_2O_5}$

ter, sulfates and heavy metals in the WPA are removed in the pretreatment step. Next, the iron, aluminum, and magnesium are extracted by an acidic extractant. After stripping the loaded acidic extractant by the $(NH_4)_2SO_4$ and H_2SO_4 solution, the sulfate crystals of iron, aluminum, and magnesium are obtained by crystalling in the stripping acid. Then, the activated carbon decolorization process is carried out again to remove the dissolved extractant from the purified WPA. After that, a concentration operation is added to recover fluorine resources for the production of anhydrous hydrogen fluoride and to concentrate the WPA into the wet-process superphosphoric acid (WSPA). By the way, the superphosphoric acid (SPA) is defined as phosphoric acid with a phosphorus content of 68-83% P_2O_5, which contains a certain amount of polyphosphoric acid (PPA) [16]. Finally, the WSPA enters the H_3PO_4 extraction section. After comparing tributyl phosphate (TBP), methyl isobutyl ketone (MiBK), diisopropyl ether (DiPE), and n-octyl alcohol extractants, we found that only TBP had a clear phase interface, while the rest of the extractants were partially miscible with WSPA. In addition, to maintain the fluidity of the WSPA, the extraction process needs to be carried out at a higher temperature. The high boiling point of TBP is also suitable for this process. The high phosphorus content of the WSPA will promote the extraction efficiency. Likewise, the raffinate has a high phosphorus content to enhance its utilization. It can be used to produce ammonium polyphosphate (APP) by the TVA process [17,18].

This route not only addresses the above-mentioned shortcomings in the traditional process, but also allows for the recovery of a significant amount of associated resources in the WPA. A comparison of this process with the conventional TBP purification process is shown in Table 1 [19-23]. The feasibility of the MI extraction section of the process has been verified by a pilot experiment of 1,000 tons phosphoric acid (expressed with the weight of P_2O_5)/year [24].

In the present work, the subsequent H_3PO_4 extraction process was investigated.

The extraction performance of TBP in WPA has been extensively studied, including phase equilibrium [25-31], physical properties [32], and the extraction kinetics [21]. However, the extraction of H_3PO_4 from WSPA by TBP has not been reported. The concentration gradient in this system is higher than in previous studies, which would enhance the extractant loading. A limit value of the H_3PO_4 loading that meets the purification requirements can be obtained by controlling the extraction conditions. Also, the extraction mechanism may have changed under high H_3PO_4 loading conditions. Therefore, in this work, extraction equilibrium experiments are explored to optimize the extraction conditions. Moreover, the TBP extraction mechanism under high H_3PO_4 loading was explained via infrared spectra and Raman spectra analyses. Finally, the feasibility of the entire process was illustrated by the scrubbing and stripping experiments.

EXPERIMENTAL SECTION

1. Materials and Instruments

Phosphoric acid (H_3PO_4, >85%) and tributyl phosphate ($C_{12}H_{27}O_4P$, >98.5%) are both analytical grade reagents purchased from Chengdu Kelong Chemical Reagent Co., Ltd. Wet-process superphosphoric acid used was supplied by Tianan Chemical Co., Ltd., Yunnan, China. Superphosphoric acid (SPA, 72.8% P_2O_5) was obtained by concentrating phosphoric acid in a reduced pressure distillation unit. Ultrapure water (electrical conductivity $\leq 10^{-4}$ Sm^{-1}) was used for the experiment and chemical analysis. Sulfonated kerosene (boiling point 180-280 °C, RG) was obtained from Chengdu Kelong Chemical Reagent Co., Ltd. All chemical reagents were used without further purification. A DF-101S thermostatic oscillator (Kewei Yongxing Instrument Co., Ltd., Beijing, China) with a temperature control accuracy of ±0.1 K was used to control the equilibrium temperature. An analytical balance (FA2204N, ShangHai Jingxue Kexue Instrument Co., Ltd, Shanghai, China) was used to weigh the mass of samples with an uncertainty of ±0.0001 g.

2. Extraction Method and Procedure

The extractant was prepared by mixing TBP with sulfonated kerosene in a designed volume ratio and was equilibrated with water to achieve a saturated water content. The WSPA and extractant were mixed in a 500 mL breaker basing the desired proportion and preheated to the extraction temperature. Then, the sealed beaker was placed in a water bath oscillator to maintain the temperature. At this point, the extraction reaction began, and the mixture was stirred for the desired time. The mixture remained stationary in the water bath until a complete separation of the extract and raffinate phases. Then, it was transferred to a separatory funnel to precisely separate the raffinate. The extract phase was centrifuged at a set centrifugal speed to remove physical entrainment altogether. A balance accurately weighed the mass of the organic phase (accurate to 0.01 g).

Then, the organic phase was mixed with water at R_0=2, T=80 °C for 10 mins. After being thoroughly mixed and phase stabilized, it was transferred to a separatory funnel to separate the two phases. The aqueous phase was collected in a 1 L collection flask, while the organic phase continued to be mixed with ultrapure water. Finally, the operation was repeated three times in the same way. It was verified by pre-experiment that all extracts from the loaded organic phase went into the collected aqueous phase after four stripping times (Fig. S1). The final collected aqueous phase was weighed (accurate to 0.01 g), and the samples were retained for analysis of P, Fe, Al, Mg, and Ca according to the corresponding method in Section 2.3. The species in the extract phase and raffinate phase were obtained by mass balance. Ostwald-Sprenge-type pycnometers determined the density of raffinate and loading extractant at a specific temperature with a bulb of 10 cm^3 and an internal capillary with a diameter of 1 mm [26]. Thus, the volume of the two phases could be calculated from density and mass.

The extraction rate E_i, distribution ratio D_i, and selectivity coefficient b_i for component *i* are defined by Eqs. (1)-(3), respectively [11].

$$E_i = \frac{\text{mass of the extracted } i \text{ in organic phase}}{\text{total mass of the component } i \text{ in feedstock}} = \frac{\text{mass of the component } i \text{ in final collected aqueous phase}}{\text{total mass of the component } i \text{ in feedstock}} = \frac{m_{aq}^{tl} \cdot w(i)_{aq}^{tl}}{m_f \cdot w(i)_f} \quad (1)$$

$$D_i = \frac{C_i^{org}}{C_i^{ino}} \quad (2)$$

$$\beta_{i/j} = \frac{D_i}{D_j} = \frac{C_i^{org}/C_i^{ino}}{C_j^{org}/C_j^{ino}} = \frac{n_i^{org}/n_i^{ino}}{n_j^{org}/n_j^{ino}} \cdot \frac{V^{org}/V^{ino}}{V^{org}/V^{ino}} = \frac{n_i^{org}/n_i^{ino}}{n_j^{org}/n_j^{ino}} = \frac{m_i^{org}/m_i^{ino}}{m_j^{org}/m_j^{ino}} = \frac{w_i^{org}/w_i^{ino}}{w_j^{org}/w_j^{ino}} \cdot \frac{m^{org}/m^{ino}}{m^{org}/m^{ino}} = \frac{w_i^{org}/w_i^{ino}}{w_j^{org}/w_j^{ino}} \quad (3)$$

3. Analysis and Characterization

The mass fraction of P in samples was analyzed by the phosphomolybdate quinoline gravimetric method [27]. Fe, Al, Mg, and Ca contents were determined by an inductively coupled plasma optical emission spectrometer (PerkinElmer, ICP-OES 7000DV). The mass fraction of H_2O in the organic phase was measured by a Karl Fischer moisture titrator (AFK-1B, Shanghai HOGON Scientific Instrument Co., Ltd) [11]. A DIONEX ICS-600 chromatography system with an AS50 automated sampler and an ED50 electrochemical detector was used for phosphorus speciation analysis [16]. As shown in Table 2, phosphates with different degrees of polymerization in the sample can be effectively analyzed depending on the residence time. TBP, kerosene, ultrapure water and SPA were mixed thoroughly in the desired ratio for spectroscopic determination. The infrared spectrum was measured by an infrared spectrometer (Mettler Toledo, ReactIR). Raman spectra were recorded using laser Raman spectroscopy (HORIBA, LabRAM HR, France) at an excitation wavelength of 532 nm.

To express the H_3PO_4 loading ratio of TBP, the LRP value is defined as Eq. (4).

$$LRP(\%) = \frac{m_{H_3PO_4}^{org}}{m_{H_3PO_4}^{org} + m_{TBP}^{org}} \times 100 \quad (4)$$

Table 2. Residence time distribution of phosphate at different polymerization levels [16]

Phosphorus species	Abbreviation	Peak position (min)
PO_4^{3-}	P_1	4.597
$P_2O_7^{4-}$	P_2	6.350
$P_3O_9^{3-}$	P_{3m}*	6.663
$P_3O_{10}^{5-}$	P_3	7.303
$P_4O_{13}^{6-}$	P_4	8.313
$P_5O_{16}^{7-}$	P_5	9.137
$P_6O_{19}^{8-}$	P_6	9.743
$P_7O_{22}^{9-}$	P_7	10.453
$P_8O_{25}^{10-}$	P_8	11.227
$P_9O_{28}^{11-}$	P_9	12.090
$P_{10}O_{31}^{12-}$	P_{10}	13.290

P_{3m}*: trimetaphosphate

The LRP value can be converted into the molar ratio of H_3PO_4 to TBP (k).

$$k=\frac{n_{H_3PO_4}}{n_{TBP}}=2.718\left(\frac{LRP}{1-LRP}\right) \quad (5)$$

RESULTS AND DISCUSSION

1. Raw Material Analysis

WSPA and SPA are the raw materials for subsequent equilibrium and characterization experiments, respectively. The phosphorus speciation analysis of the WSPA and the SPA is shown in Fig. 2. The results show that the WSPA contains 86.06% PO_4^{3-}, 11.62% $P_2O_7^{4-}$, and 2.3% $P_3O_{10}^{5-}$, while the SPA contains 98.12% PO_4^{3-} and 1.88% $P_2O_7^{4-}$. The PPA distribution behavior of WSPA in the two phases is explored in Fig. S2, and results show that PPA was completely hydrolyzed at a high extraction temperature. Thus, we only need to pay attention to the H_3PO_4 extraction equilibrium. The components of the WSPA are shown in Table 3. In addition, small amounts of PPA in SPA were neglected in the spectral characterization experiments.

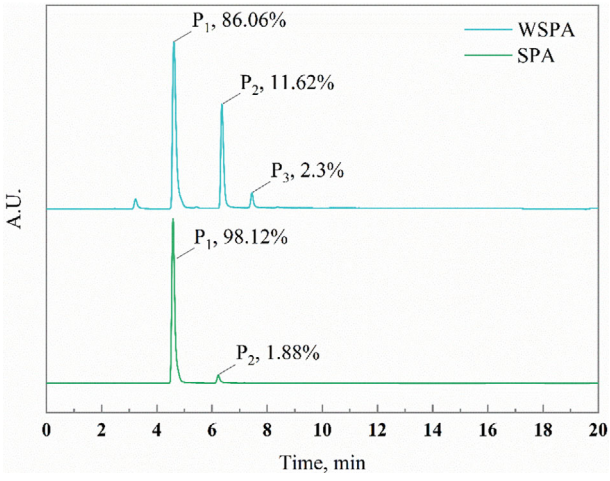

Fig. 2. The polyphosphoric acid constitution in WSPA and SPA.

Table 3. The composition of WSPA

Component	P_2O_5	Fe_2O_3	Al_2O_3	MgO	CaO	MER
w(%)	71.21	0.694	0.774	0.349	0.997	0.026

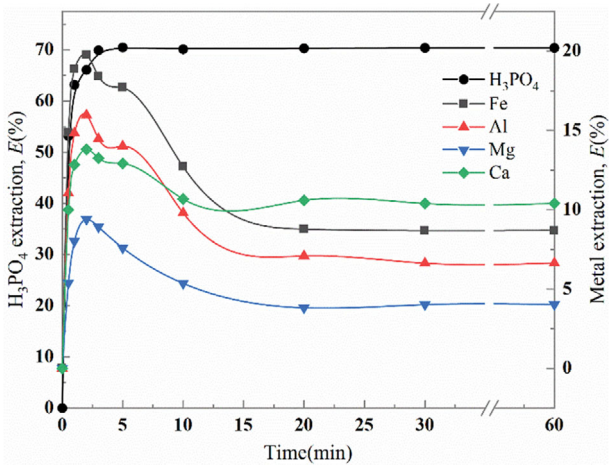

Fig. 3. Effect of the extraction time on the H_3PO_4, Fe, Al, Mg, and Ca extraction rate. R_0=6, stirring rate=300 rpm (linear velocity=0.785 m/s), φ_{TBP}=80%, T=80 °C, centrifugal speed=3,000 rpm (5,205.4 g), centrifugal time=10 min.

2. Extraction Equilibrium Experiment

2-1. Effect of Extraction Time

To ensure that equilibrium was reached for all experiments in this study, it was necessary to determine an adequate extraction time. Fig. 3 shows the variation of the extraction rate over time from 0-60 minutes. The extraction rate of H_3PO_4 reached a maximum of 70.40% at 4 min and remained stable thereafter, which means that the extraction process of H_3PO_4 could be completed in a short 4 mins mixing. However, the equilibrium time for metal ions was longer. The Fe, Al, Mg, and Ca extraction rate was 14.87%, 11.05%, 5.39%, 9.99% at 0.5 min, respectively, reaching maximum values of 19.76%, 15.98%, 9.39%, 13.81% at 2 min, and stabilizing at 7.38%, 6.63%, 4.02%, 11.79% after 20 min. The results indicate that TBP has a good extraction capability and selectivity for H_3PO_4 from WSPA, and the extraction equilibrium time for metal ions is five times longer than that of H_3PO_4. Therefore, in the subsequent experiments, the appropriate equilibration time was selected as 30 mins. The appearance of a peak in the extraction rate of metal ions versus time is a curious phenomenon, which suggests that the metal ions are extracted first into the organic phase and then out of it. The phenomenon will be explained later in the following.

2-2. Effect of Centrifugal Speed of Extract Phase

The high viscosity of WSPA and TBP can cause physical entrapment in the extract phase. To ensure complete separation of the two phases at the end of the extraction reaction, experiments were carried out on the effect of different centrifugal speeds on the content of metal ions in the extract phase. The results are shown in Fig. 4. After centrifugation speed greater than 2,000 rpm (3,470.3 g), the content of metal ions was stabilized and two phases were wholly

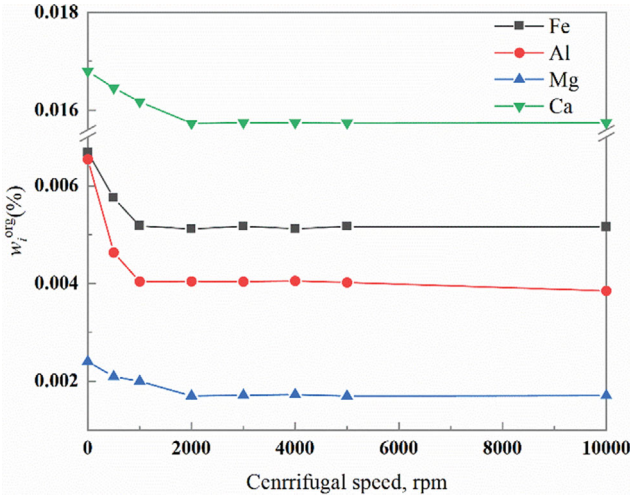

Fig. 4. Effect of centrifugal speed on the content of metal ions in organic phase. R_0=6, stirring rate=300 rpm (linear velocity= 0.785 m/s), φ_{TBP}=80%, T=80 °C, centrifugal time=10 min, extraction time=30 min.

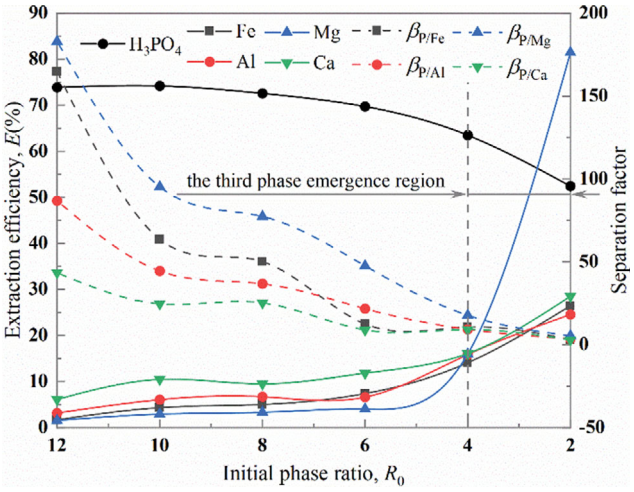

Fig. 5. Effect of the initial phase ratio R_0 on the H_3PO_4, Fe, Al, Mg, and Ca extraction rate. Stirring rate=300 rpm (linear velocity= 0.785 m/s), φ_{TBP}=80%, T=80 °C, centrifugal speed=3,000 rpm (5,205.4 g), Centrifugal time=10 min, extraction time=30 min.

separated. Therefore, the centrifugation speed was fixed at 3,000 rpm (5,205.4 g) in the experiments.

2-3. Effect of Initial Phase Ratio R_0

The effect of the initial phase ratio R_0 ($R_0=V_0^{org}/V_0^{aq}$) on H_3PO_4 extraction behavior was investigated under T=80 °C and φ_{TBP}= 80%; the results are presented in Fig. 5. The general trend of the extraction rate of H_3PO_4 decreased slightly with the decrease of R_0, while the extraction rate of the metal ions initially gently changed and after $R_0 \leq 4$ rose rapidly. The H_3PO_4 extraction rate was maintained at around 70% at different R_0, and an increase in R_0 promoted a higher selectivity of H_3PO_4. In addition, the organic phase split into a light kerosene-rich phase and a heavy TBP-rich phase in the experiments with R_0=4 and 2. This phenomenon is not conducive to large-scale industrial extraction because it causes "flooding to interfere with the continuous counter-current extraction process [33]. To maximize the H_3PO_4 loading of the extractant and avoid the third phase appearance, R_0 was determined to be 6 in subsequent experiments.

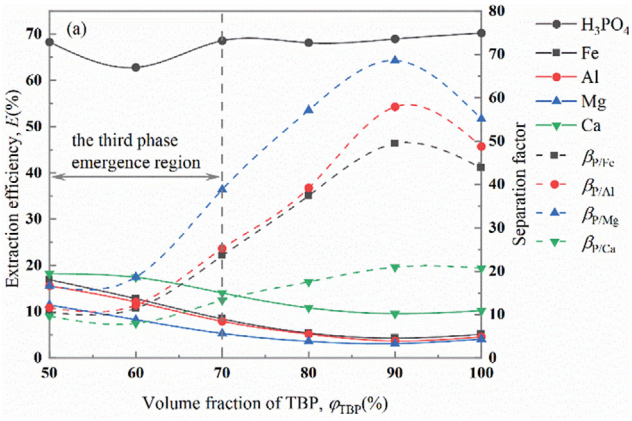

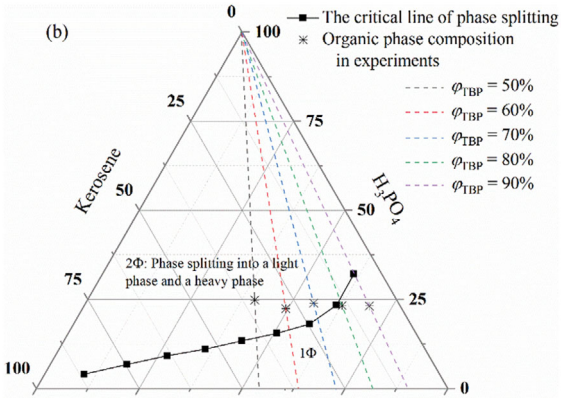

Fig. 6. (a) Effect of the TBP concentration on the H_3PO_4, Fe, Al, Mg and Ca extraction. R_0=6, stirring rate=300 rpm (linear velocity=0.785 m/s), T=80 °C, centrifugal speed=3,000 rpm (5,205.4 g), centrifugal time=10 min, extraction time=30 min. (b) Liquid-liquid equilibria for the system Kerosene-H_3PO_4-TBP at 80 °C.

2-4. Effect of TBP Concentration

The effect of TBP concentration on the extraction rate of H_3PO_4 was investigated. Fig. 6(a) shows that the variation of φ_{TBP} has little effect on the H_3PO_4 extraction rate, but it favors the separation factor of H_3PO_4 and achieves optimal results at φ_{TBP}=90%. When φ_{TBP} is less than 70%, the third phase also appears. In fact, despite the similar H_3PO_4 extraction rate, the extract phase was in different loading states. For example, the TBP concentration doubled from φ_{TBP}=50% to 100%, but the extraction rate only increased by 1.93%. While the separation factors for P/Fe, P/Al, P/Mg, P/Ca varied significantly from 10.57, 11.64, 16.60, 9.67 to 43.83, 48.79, 55.13, 20.73, respectively. The molar ratio k of H_3PO_4 to TBP in the extract phase can be calculated as 1.66 (φ_{TBP}=50%) and 0.82 (φ_{TBP}=100%), respectively. It can be concluded that the higher the H_3PO_4 loading of TBP, the lower the H_3PO_4 selectivity, and the third phase will appear after exceeding a critical loading value [34].

The ternary organic phase diagram of Kerosene-H_3PO_4-TBP at 80 °C is shown in Fig. 6(b) for predicting the critical value of third

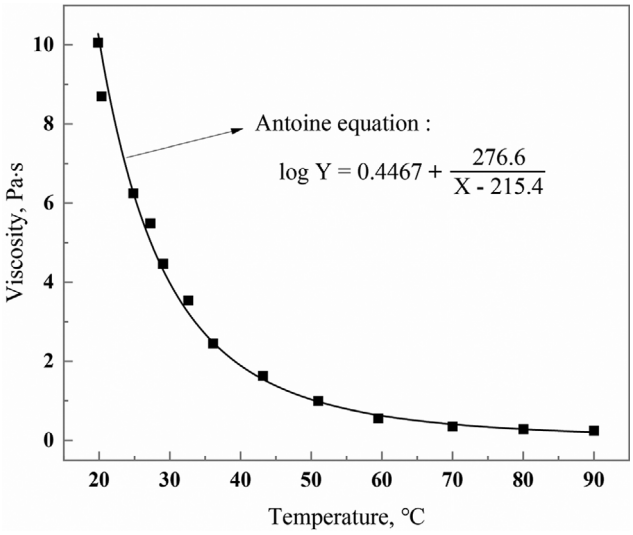

Fig. 7. The effect of temperature on the viscosity of WSPA.

phase formation at different TBP concentration conditions. The critical lines for phase splitting are given in the diagram. The constituent points above the critical line are in the two-phase region, representing the splitting of the organic phase into light and heavy phases. While the constituent points below the critical line are in the single-phase region, representing regular molecular solutions. After importing the organic phase composition data into the phase diagram, the predicted results are well consistent with the experimental phenomena.

In this work, the third phase is expected to be avoided, and a high H_3PO_4 loading in the organic phase should be maintained. Meanwhile, the phase separation time for stripping increases significantly at φ_{TBP}=90% and 100%. Therefore, 80% of φ_{TBP} was chosen as the optimal TBP concentration.

2-5. Effect of Temperature

Temperature controls the viscosity of the WSPA, which is an indicator of mass transfer performance. As is shown in Fig. 7, the viscosity of WSPA is very sensitive to temperature, and 50-100 °C was selected as a suitable temperature range for the extraction experiments.

The extraction results are shown in Fig. 8(a). A slight decrease in the extraction rate of H_3PO_4 occurred as the temperature increased, indicating that H_3PO_4 extraction under this condition is weakly exothermic. The equation for converting the extraction rate E_i into the distribution ratio D_i is shown in Eq. (6). According to Eq. (7), the experimental point is fitted by the van't Hoff equation, and the enthalpy of the extraction process is calculated from the slope of the fitting line [3]. As is shown in Fig. 8(b), the enthalpy is −1.3 kJ/mol, which is much lower than the enthalpy with (ΔH_1= −16.39 kJ/mol) or without (ΔH_2=−22.53 kJ/mol) $CaCl_2$ obtained by Zhang [11]. It implies that the H_3PO_4 enters the organic phase not by a direct reaction with TBP but by a weaker bond. Reasonable speculation is that the H_3PO_4 molecules form an intermolecular hydrogen bond with the extraction complex in the extract phase. In view of the solvent evaporation and the H_3PO_4 selectivity, a suitable temperature of 353.2 K was chosen.

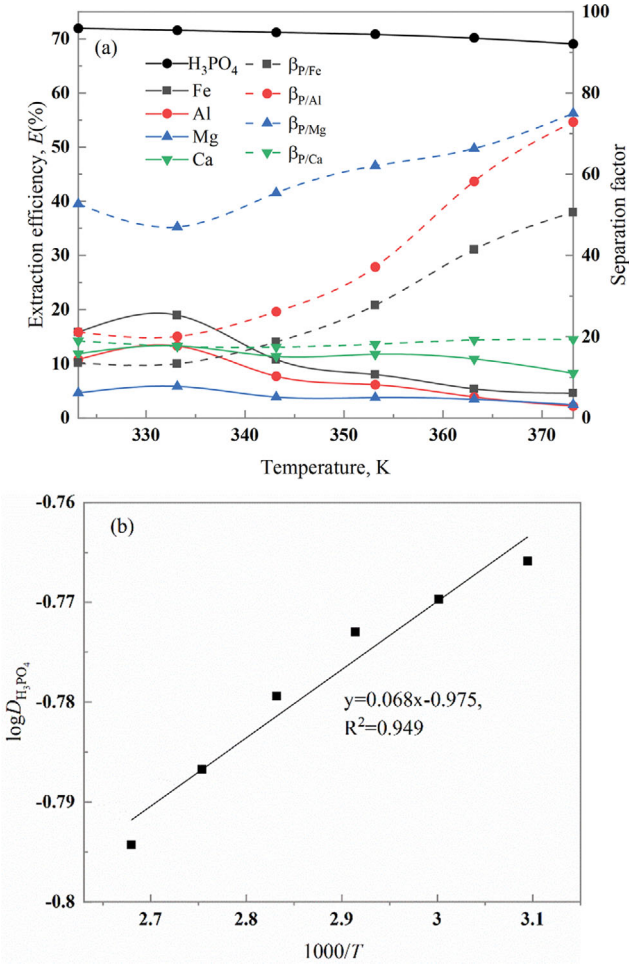

Fig. 8. (a) Effect of the temperature on the H_3PO_4, Fe, Al, Mg and Ca extraction. R_0=6, stirring rate=300 rpm (linear velocity= 0.785 m/s), φ_{TBP}=80%, T=353.2 K, extraction time=30 min, centrifugal speed=3,000 rpm (5,205.4 g), centrifugal time= 10 min, extraction time=30 min. (b) Linear fitting of log $D_{H_3PO_4}$ to 1,000/T.

$$D_i = \frac{E_i}{R_e(1-E_i)} \quad (6)$$

$$\log D_i = \frac{\Delta H}{2.303RT}\frac{1}{T} + C \quad (7)$$

2-6. The Crosscurrent Multi-stage Extraction Experiment

Fig. 9 shows the effect of the crosscurrent extraction stages on the H_3PO_4 and metal ion extraction rate. After two stages, the total extraction rate of H_3PO_4 and metal ions becomes stable. The maximum extraction rate of H_3PO_4, Fe, Al, Mg, and Ca is 82.4%, 6.76%, 5.63%, 3.40%, and 11.46%, respectively. The highest MER value for the raffinate was 0.173 and it contains 63.5% P_2O_5. It is in a solid state after cooling, which makes them easy to transport when utilized.

From the previous equilibrium experiments, the optimized conditions for the extraction were R_0=6, T=323.5 K, and φ_{TBP}=80%. Under these conditions, 70.0% H_3PO_4, 7.38% Fe, 6.64% Al, 4.02% Mg, and 11.80% Ca were extracted in a single stage. Moreover, the

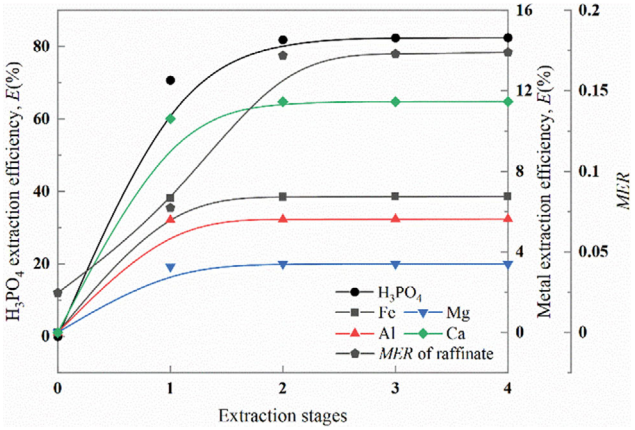

Fig. 9. The results of cross-current multi-stage extraction experiment. R_0=6, stirring rate=300 rpm (linear velocity=0.785 m/s), φ_{TBP}=80%, T=80 °C, centrifugal speed=3,000 rpm (5,205.4 g), centrifugal time=10 min, extraction time=30 min.

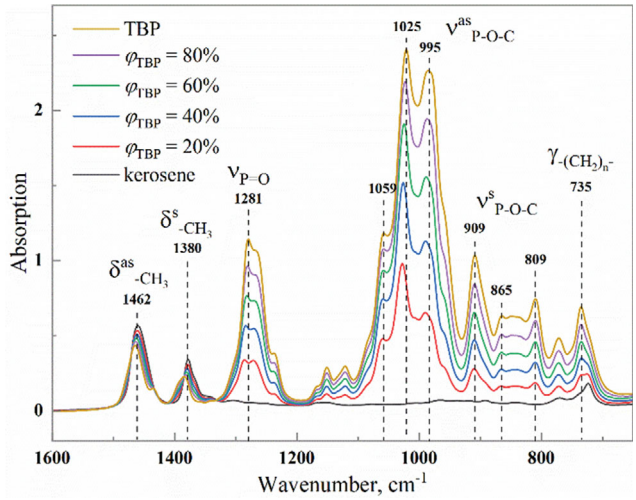

Fig. 10. The FT-IR spectra of kerosene, TBP, and different volume fractions of TBP solutions diluted by kerosene.

separation factors of $\beta_{P/Fe}$, $\beta_{P/Al}$, $\beta_{P/Mg}$, and $\beta_{P/Ca}$ were 12.48, 21.66, 47.57, and 8.89, respectively. In addition, the following three anomalies emerged compared to the conventional aqueous-organic phase extraction. (1) In the effect of extraction time, the metal ions enter the extract phase first and come out later; (2) The absolute value of the enthalpy change under high loading conditions is smaller than the results of others; (3) After exceeding a loading threshold, the third phase appeared. These phenomena suggest that the mechanism of H_3PO_4 extraction from WSPA by TBP has changed compared to the low H_3PO_4 concentration studies [11,28]. Similar features are also mentioned in the studies of Dhouib-Sahnoun [25], Tedesco [35], and Higgins [36], with speculation that aggregates are formed during the extraction process. Nave et al. [37] studied the supramolecular organization of TBP in organic diluent on approaching the third phase transition, using TBP extract HNO_3 as an example. The results indicate that the extraction complexes of TBP·HNO_3 form aggregates and the interactions between the aggregates dominate the formation of the third phase. In this study, we also attribute this to the formation of reverse micelles (RMs) by polymerization of the extraction complex. From this speculation, the previous phenomena can be explained. When the extractant and WSPA come into contact, the locally excessive H_3PO_4 concentration in the extract phase leads to the formation of RMs and the metal ions enter the organic phase through the polar core of the RMs. As the system becomes homogeneous, the RMs break up and release the metal ions again. The H_3PO_4 molecule in the polar core is not directly bound to the TBP; thus the enthalpy change of the H_3PO_4 extraction process is small. Eventually, as the RMs grow, the core spacing of the RMs is shortened and mutual attraction leads to the formation of a third phase. To further test the speculation, the formation process of aggregates is further characterized microscopically by Fourier transform infrared (FT-IR) and Raman spectroscopy.

3. The Extraction Mechanism

3-1. FT-IR Analysis

The infrared spectra of kerosene and TBP are shown in Fig. 10. The corresponding structures can be identified by the position, shape, and intensity of these peaks. The asymmetrical and symmetrical deformation vibration of CH_3- appears at 1,462 and 1,380 cm^{-1}, respectively, and the peak at 735 cm^{-1} can be attributed to the out-of-plane bending vibration of -$(CH_2)_n$- [38-41]. These structures were found in the spectra of both TBP and kerosene. Additionally, several distinct peaks only appear in the spectrum of TBP. The peak at 1,281 cm^{-1} is the characteristic absorption of the P=O bond, which is close to the typical absorption of the P=O bond in alkyl phosphate esters. The peaks at 1,025/995 cm^{-1} and 865/809 cm^{-1} can be attributed to the asymmetrical and symmetrical stretching vibration of P-O-C, respectively. In fact, the absorption peak of P-O-C is widely reported in phosphate ester extractants. The peak intensity of the C-O bond is stronger than the P-O bond in the symmetrical stretching vibration region of 1,060-975 cm^{-1}, while in the asymmetrical stretching vibration region of 865-805 cm^{-1} the law is the opposite. Finally, There is also a peak at 909 cm^{-1} that is not found in trimethyl phosphate and triethyl phosphate. The peak appears in tripropyl phosphate and becomes stronger in tributyl phosphate. It is speculated that the peak was the splitting peak of the asymmetric stretching vibration of the P-O bond.

Based on the results of the peak fitting, the peak position of P=O, P=O···H_2O, and P=O···H_3PO_4 was determined to be 1,283, 1,267 and 1,233 cm^{-1}, respectively (Support Information). Furthermore, the infrared spectra of extractants (φ_{TBP}=80%) at different H_3PO_4 loadings were analyzed to elucidate the molecular behavior of TBP during the H_3PO_4 extraction process. From the extraction equilibrium experiments, it is known that phase separation occurs when the H_3PO_4 loading of the extractant exceeds the critical value. Therefore, ten equidistant loading points were selected for analysis, which included the points where the third phase appeared or not. As shown in Fig. 11, the loaded organic phase is a homogeneous organic phase in the experimental points with LRP values below 28%. The phase splits into a light and heavy phase with LRP values above 28%. LRP=28% is very close to the critical point, and a slight phase splitting was also observed. Thus, if phase separation occurred, the light and heavy phases were analyzed separately. The spectral results are shown in Fig. 12. As predicted, the signals of

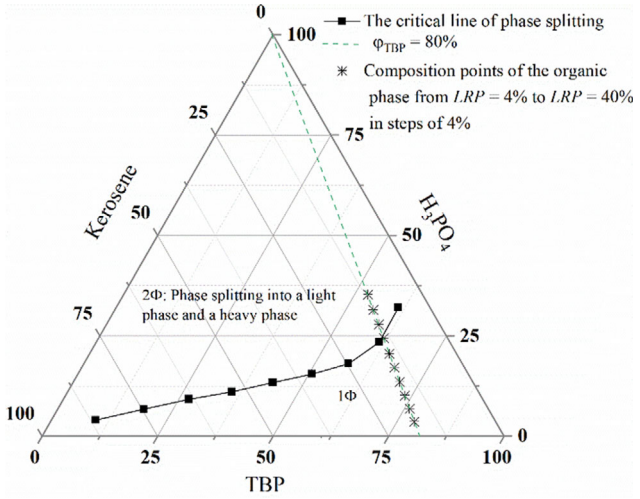

Fig. 11. Composition of Infrared spectroscopy test points for semi-quantitative analysis.

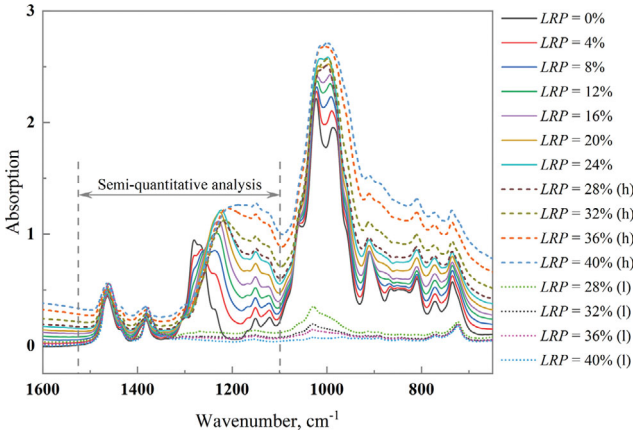

Fig. 12. The infrared spectra of the extractant loaded with different amounts of H_3PO_4 ("h" is for heavy phase, "l" is for light phase).

TBP and H_3PO_4 molecules are dominant in the heavy phase, while the signals of kerosene and a small amount of TBP molecules are dominant in the light phase. In the light phase, the TBP signal diminishes with increasing the LRP value from 28% to 40%, representing a decrease in TBP molecules.

The peak area of the characteristic functional groups is used for semi-quantitative analysis of the relative content of the corresponding chemical structures of the extraction complex. The deformation vibration region of CH_3- is chosen as the standard internal peak of the system, related to the concentration of TBP and kerosene. And three functional group indexes are defined as shown in Eq. (8)-(11) [42]:

$$I_{P=O} = A_{1283}/\Sigma A \quad (8)$$

$$I_{P=O\ldots H_2O} = A_{1267}/\Sigma A \quad (9)$$

$$I_{P=O\ldots H_3PO_4} = A_{1223}/\Sigma A \quad (10)$$

$$\Sigma A = A_{1233} + A_{1267} + A_{1283} + A_{1382} + A_{1396} + A_{1434} + A_{1463} \quad (11)$$

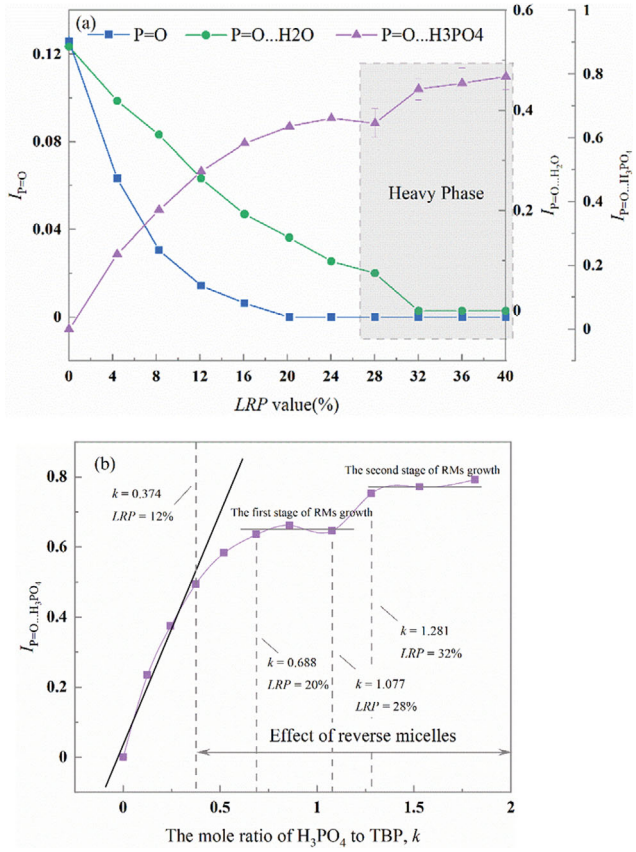

Fig. 13. (a) The $I_{P=O}$, $I_{P=O\ldots H_2O}$, and $I_{P=O\ldots H_3PO_4}$ versus LRP value. (b) The $I_{P=O\ldots H_3PO_4}$ versus the mole ratio k of H_3PO_4 to TBP.

As shown in Fig. 13(a), the $I_{P=O}$, $I_{P=O\ldots H_2O}$, and $I_{P=O\ldots H_3PO_4}$ can be calculated from the TBP spectral fitting results of LRP=0 to 40% (Table 4). Fig. 13(a) reflects the variation in the relative content of the three P=O peaks. As the LRP value increases, the $I_{P=O\ldots H_3PO_4}$ increases gradually and stabilizes in the LRP=20-28% region. When the LRP value is located in the heavy phase region, the $I_{P=O\ldots H_3PO_4}$ shows a "stepwise" and then stabilizes again. While the $I_{P=O}$ and $I_{P=O\ldots H_2O}$ decreased simultaneously and reached the lowest values at LRP=20% and LRP=32%, respectively. It implies that the H_3PO_4 molecule enters the organic phase partly by binding to the "free" P=O and partly by displacing the bound H_2O from the P=O⋯H_2O. Phase splitting increases the concentration of TBP and H_3PO_4, which leads to the stepwise performance of $I_{P=O\ldots H_3PO_4}$ and $I_{P=O\ldots H_2O}$. In addition, from the perspective of the variation rate of the functional group indexes, the decrease rate of $I_{P=O}$ is greater than that of the $I_{P=O\ldots H_2O}$, which indicates that H_3PO_4 preferentially combines with the "free" P=O.

Moreover, if the H_3PO_4 molecular entered the organic phase through Eq. (12) and Eq. (13) only, the $I_{P=O\ldots H_3PO_4}$ should be linearly related to the molar ratio of H_3PO_4 to TBP. Thus, according to Eq. (5), the LRP value is transformed into the mole ratio, k, and the results are shown in Fig. 13(b). The $I_{P=O\ldots H_3PO_4}$ is consistent with the predicted results when the molar ratio k is less than 0.374. However, a significant "negative deviation" is observed when the molar ratio k is greater than 0.374. Even a "plateau" appears for a

Table 4. The fitting results of LRP=0 to 40%

LRP value (%)	Parameters	Peak1	Peak2	Peak3	Peak4	Peak5	Peak6	Peak7	R^2
0	X_c	-	1,266.06	1,283.42	1,382.49	1,396.76	1,434.07	1,463.38	0.9999
	A	-	27.21	6.49	3.39	0.74	1.19	12.57	
	FWHH	-	30.47	13.83	18.14	11.44	13.79	28.62	
4	X_c	1,233.46	1,266.76	1,283.79	1,382.34	1,397.02	1,434.10	1,463.41	0.9999
	A	14.40	25.69	3.87	3.22	0.73	1.20	12.20	
	FWHH	43.12	33.93	12.89	18.18	11.60	13.88	28.45	
8	X_c	1,233.46	1,267.55	1,284.22	1,382.22	1,397.14	1,434.14	1,463.46	0.9998
	A	25.64	24.12	2.10	3.02	0.72	1.18	11.85	
	FWHH	44.71	37.93	11.82	18.03	11.72	13.88	28.36	
12	X_c	1,233.46	1,267.55	1,284.22	1,382.08	1,397.20	1,434.19	1,463.51	0.9997
	A	35.16	18.79	1.03	2.80	0.73	1.17	11.47	
	FWHH	48.55	38.34	10.69	17.71	11.88	13.93	28.25	
16	X_c	1,233.46	1,267.55	1,284.22	1,382.02	1,397.36	1,434.24	1,463.57	0.9990
	A	41.58	13.75	0.46	2.64	0.70	1.18	11.04	
	FWHH	48.55	38.34	10.69	17.65	11.92	14.22	28.08	
20	X_c	1,233.46	1,267.55	-	1,382.04	1,397.41	1,434.37	1,463.60	0.9969
	A	43.21	9.93	-	2.49	0.65	1.15	10.57	
	FWHH	48.55	38.34	-	17.60	11.64	14.27	27.81	
24	X_c	1,232.29	1,267.62	-	1,382.11	1,397.53	1,434.47	1,463.62	0.9963
	A	39.08	5.85	-	2.38	0.60	1.13	10.04	
	FWHH	50.27	28.37	-	17.77	11.43	14.52	27.49	
28 (heavy phase)	X_c	1,232.29	1,267.62	-	1,381.43	1,397.70	1,435.22	1,463.14	0.9962
	A	32.34	3.77	-	2.47	0.46	1.20	9.83	
	FWHH	51.89	26.08	-	18.35	10.75	16.14	26.91	
32 (heavy phase)	X_c	1,232.29	-	-	1,381.70	1,397.68	1,435.17	1,463.35	0.9962
	A	39.57	-	-	2.23	0.43	1.16	9.18	
	FWHH	68.04	-	-	18.13	10.77	16.10	26.77	
36 (heavy phase)	X_c	1,232.29	-	-	1,382.19	1,397.35	1,434.96	1,463.78	0.9962
	A	39.31	-	-	1.86	0.45	1.08	8.27	
	FWHH	71.78	-	-	17.07	11.10	15.66	26.49	
40 (heavy phase)	X_c	1,232.29	-	-	1,382.68	1,397.18	1,434.89	1,464.22	0.9962
	A	39.31	-	-	1.54	0.43	1.01	7.35	
	FWHH	71.78	-	-	16.30	11.26	15.44	26.12	

Note: 1. X_c, A, and FWHH represent the peak location, area, and full width at half maxima; 2. Each point was repeated three times, and their average was taken as the final result.

molar ratio k greater than 0.688. In fact, these phenomena are evidence of self-polymerization of the extraction complex TBP·H_3PO_4 to form RMs, which means that a part of H_3PO_4 molecules enters the organic phase by entering the polarity core of the RMs. The critical micelle concentration (CMC) of TBP·H_3PO_4 can be determined as the concentration corresponding to k=0.374. Additionally, the apparent broadening of the error bars of $I_{P=O\ldots H_3PO_4}$ in the heavy phase is indicative of the inhomogeneity of the system on the molecular scale, which is another evidence of the formation of RMs.

$$H_3PO_{4aq}+TBP_{org}\rightarrow TBP\cdot H_3PO_{4org} \quad (12)$$

$$H_3PO_{4aq}+TBP\cdot H_2O_{org}\rightarrow TBP\cdot H_3PO_{4org}+H_2O_{aq} \quad (13)$$

In short, the introduction of the speculation of the formation of RMs can reasonably explain the experimental results of the semi-quantitative analysis. First, in the k=0-0.374 region, two reactions of TBP with H_3PO_4 occur according to Eq. (13) and Eq. (14). Secondly, in the k=0.374-0.688 region, the concentration of the formed extraction complex TBP·H_3PO_4 reaches the critical micelle concentration (CMC) and undergoes self-polymerization. Then, in the k=0.688-1.077 region, the $I_{P=O\ldots H_3PO_4}$ remains constant, and the H_3PO_4 molecular enter the organic phase by entering the polarity core of the RMs. Meanwhile, the entry of H_3PO_4 molecular causes the RMs to start growing larger (the first stage of RMs growth). Next, the growth of RMs could reduce the distance, and the mutual attraction of polarity cores between RMs leads to phase splitting. Therefore, a third phase is observed when k is greater than or equal to 1.077. Finally, after phase splitting, the H_3PO_4 molecular can still enter the heavy phase through the regrowth of RMs (the second

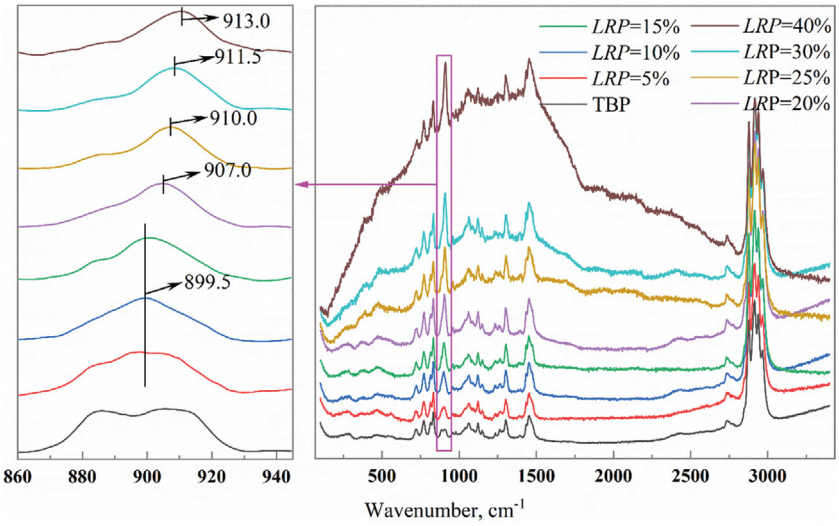

Fig. 14. Raman spectra at different LRP values.

Table 5. Raman data of the PO_4 modes of H_3PO_4 (aq) [43]

X_c/cm^{-1}	Intensity	FWHH/cm^{-1}	Assignment
357	1.3	45	ρ(O=P(OH)$_3$)
394.5	3.4	60	δ_{as}(P-(OH)$_3$)
499	9.3	54	δ_s(P-(OH)$_3$)
890.1	100	19.5	ν_s(P-(OH)$_3$)
1,008	0.9	18	ν_{as}(P-(OH)$_3$)
1,178	22.5	53	ν(P=O)
1,255	2	40	δ(PO-H)

stage of RMs growth).

3-2. Raman Analysis

Focusing on the H_3PO_4 molecule, the extraction process was analyzed by Raman spectral, and the results are shown in Fig. 14. The H_3PO_4 molecule has Raman activity, and the corresponding peaks for different vibration structures are shown in Table 5 from Rudolph's study [43]. 890.1 cm^{-1} is the most substantial peak of the H_3PO_4 molecule corresponding to ν_s(P-(OH)$_3$). When the H_3PO_4 molecule combines with TBP to form P=O···H_3PO_4, the peak of ν_sP(OH)$_3$ undergoes a redshift to 899.5 cm^{-1}. However, the peak of ν_s(P-(OH)$_3$) shifts further when the LRP value exceeds 15%. Rudolph proposed that when P-(OH)$_3$ forms a hydrogen bond, the protons are somewhat weakened, and the stretching mode, ν_s(P-(OH)$_3$), shows noticeably π-bonding contributions, so higher stretching peak positions are observed as normally considered with the normal P-O single bonds. Therefore, in this study, hydrogen bonds between H_3PO_4 and H_3PO_4 molecules appear in the organic phase after the LRP value greater than 15%. Thus, H_3PO_4 molecules form H_3PO_4···H_3PO_4·TBP with extraction complex H_3PO_4·TBP in the polarity core of RMs. This is also evidence of the formation of RMs.

4. Scrubbing

In this section, the purified phosphoric acid solution was used as a scrubbing solution to remove the metal ions from the extract phase. And the H_3PO_4 concentration in equilibrium with the extract phase was previously determined from the equilibrium isotherm,

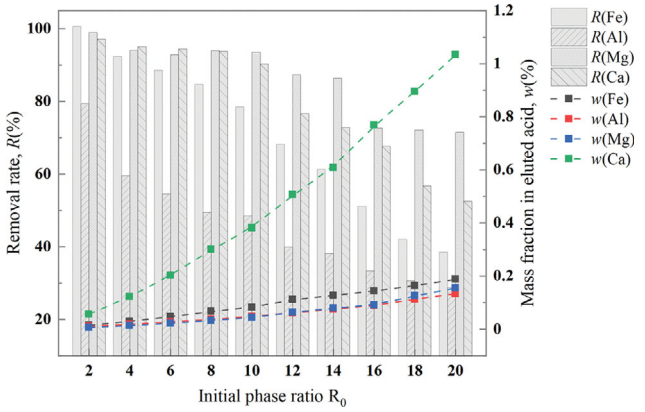

Fig. 15. Removal rate of metal ions by scrubbing under different R_0 conditions. Stirring rate=300 rpm (linear velocity=0.785 m/s), φ_{TBP}=80%, w$(P_2O_5)_{scrubbing\ sollution}$=50.47% w$(P_2O_5)_{org}$=15.03%, w(Fe)$_{org}$=0.007%, w(Al)$_{org}$=0.005%, w(Mg)$_{org}$=0.002%, w(Ca)$_{org}$ =0.028%, T=80 °C, and scrubbing time=10 min.

as shown in Fig. 18. According to Fig. 15, the overall removal rate of metal ions decreases with increasing R_0, and the removal rate of Fe, Mg, and Ca is better than that of Al. The appropriate R_0 can be chosen as 10, where the removal rate of Fe, Al, Mg, and Ca is 78.47%, 48.53%, 93.56%, 90.29%, respectively. In addition, the mass fraction of metal ions in the eluted acid tends to increase significantly with increasing R_0 and does not reach saturation values. The metal ions can be further removed by multi-stage counter-current scrubbing.

To predict the right number of counter-current scrubbing stages, the Al is targeted and a distribution curve is created as shown in Fig. 16. The same McCabe-Thiele analysis as in section 3.5 is also used here. The results show that two-stage countercurrent scrubbing reduces the aluminum ions in the loaded organic phase to less than 0.0015%. Further, a cascade experiment was conducted to simulate multistage countercurrent scrubbing. As illustrated in Fig. 17, L represents the aqueous phase and V represents the organic

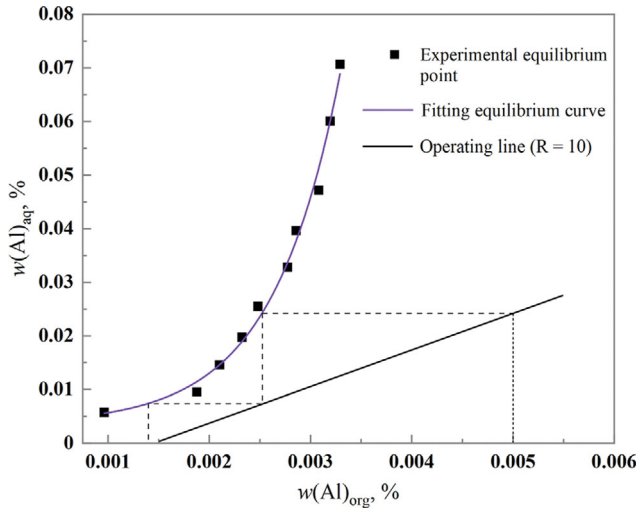

Fig. 16. Equilibrium isotherm for Al scrubbing at 80 °C. ($w(P_2O_5)_{org}$= 15.03%, $w(P_2O_5)_{scrubbing\ solution}$=50.47%).

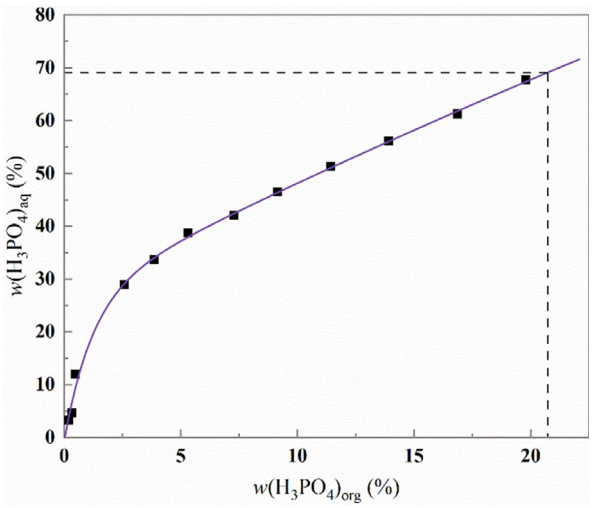

Fig. 18. Equilibrium isotherm for H_3PO_4 stripping at 80 °C.

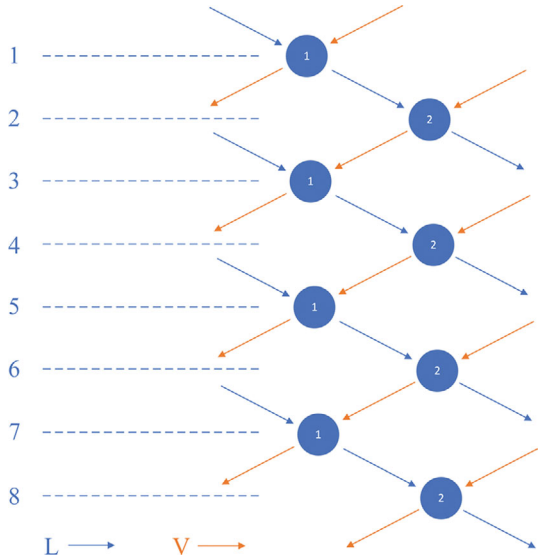

Fig. 17. Schematic diagram of the cascade experiment.

phase. The results are presented in Table 6, the first and second stages gradually stabilize as the number of rows increases, and the mass fraction of Al at stabilization is below 0.0015%. The mass fraction ratio of Fe, Al, Mg, and Ca to H_3PO_4 in the final loaded organic phase is already below the ratio in *The Chinese National Standard of GB/T 2091-2008*, which means that the industrial grade phosphoric acid product is obtained after the stripping operation [7].

5. Stripping and Stability of the Organic Phase

From Fig. 18, H_3PO_4 is capable of being stripped from the organic phase by water. However, the efficiency of single-stage stripping is low, and the large R_0 confines the concentration of the purified acid, which increases the cost of concentration. Thus, multi-stage countercurrent stripping should be considered here. McCabe-Thiele analysis was used to predict the number of theoretical stages required to complete the extraction task for a given operating condition.

H_3PO_4 molecules enter the aqueous phase from the organic phase during the continuous stripping process, resulting in a significant variation in the mass flow rate of the two phases. Therefore, the stable TBP and H_2O mass flow rate were used as reference standards in the analysis. The content of H_3PO_4 in the two phases is expressed by the mass ratio X and Y, respectively. X and Y are defined as follows.

$$Y = \frac{w(H_4PO_4)_{aq}}{w(H_2O)_{aq}} = \frac{w(H_3PO_4)_{aq}}{1 - w(H_3PO_4)_{aq}} \quad (14)$$

Table 6. The composition of the loaded extractant in cascade experiment

Row No.	P_2O_5 (wt%)	Fe (wt%)	Al (wt%)	Mg (wt%)	Ca (wt%)
0	16.08	0.0077	0.0053	0.0024	0.0379
1	16.25	0.0018	0.0033	0.0005	0.0056
2	16.16	0.0006	0.0018	0.0003	0.0023
3	16.36	0.0020	0.0034	0.0004	0.0058
4	16.15	0.0004	0.0020	0.0002	0.0020
5	16.39	0.0021	0.0027	0.0003	0.0056
6	16.10	0.0004	0.0012	0.0001	0.0016
7	16.27	0.0020	0.0028	0.0004	0.0055
8	16.13	0.0004	0.0012	0.0002	0.0014

$$X = \frac{w(H_4PO_4)_{org}}{w(TBP)_{org}} \quad (15)$$

The operating line equation is obtained from the mass balance.

$$Y_{n+1} = \frac{q(TBP)_{org}}{q(H_2O)_{aq}} X_n + \left(Y_0 - \frac{q(TBP)_{org}}{q(H_2O)_{aq}} X_r \right) \quad (16)$$

where X_n and X_r represent the mass ratio of H_3PO_4 in the organic equilibrium phase at stage n and in the regenerated extractant that completes the stripping process, respectively. Y_{n+1} and Y_0 represent the mass ratio of H_3PO_4 in the aqueous equilibrium phase at stage n+1 and in the feed of stripping water. The $q(TBP)_{org}$ and $q(H_2O)_{aq}$ are the mass flowrate of TBP in the organic phase and the mass flowrate of H_2O in the aqueous phase.

The mass flow rate ratio of $q(TBP)_{org}$ to $q(H_2O)_{aq}$ is obtained from the phase ratio in the feed stage, R_0.

$$\frac{q(TBP)_{org}}{q(H_2O)_{aq}} = \frac{\rho^{org} V_0^{org} w(TBP)_{org}}{\rho^{aq} V_0^{aq} w(H_2O)_{aq}} = R_0 \frac{\rho^{org} w(TBP)_{org}}{\rho^{aq} w(H_2O)_{aq}} \quad (17)$$

Combining Eq. (16) and Eq. (17) gives the following operation line equation:

$$Y_{n+1} = R_0 \frac{\rho^{org} w(TBP)_{org}}{\rho^{aq} w(H_2O)_{aq}} X_n + \left(Y_0 - R_0 \frac{\rho^{org} w(TBP)_{org}}{\rho^{aq} w(H_2O)_{aq}} X_r \right) \quad (18)$$

The equilibrium partition curves and operating lines at different R_0 are shown in Fig. 19. The parameters Y_0 and X_r are set to 0 and 0.02, respectively, which means that water is used as the stripping reagent and the stripping is completed when the mass ratio of H_3PO_4 to TBP in the organic phase is below 0.02. Moreover, the results emerge that the target can be reached after three stages of counter-current stripping at R_0=3.2. The results of ten extraction cycles of the extractant under the same conditions are shown in Fig. 20. Moreover, the extraction rate of H_3PO_4 keeps stable at 70% with only slight variation, indicating that the extractant has good stability in extracting H_3PO_4 from WSPA.

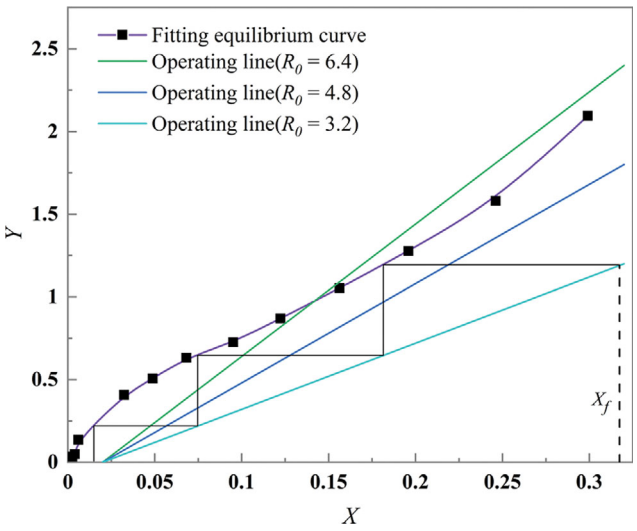

Fig. 19. Prediction of theoretical stages by McCabe-Thiele graphic method. X_r=0.02; Y_0=0; X_f=0.317; T=80 °C.

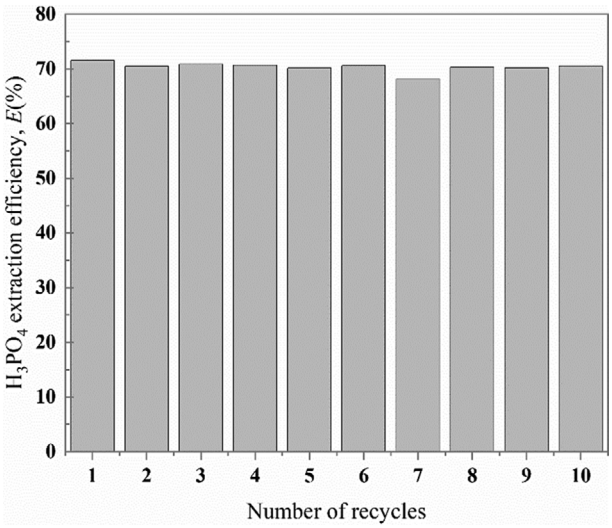

Fig. 20. Effect of the number of extractant recycles on the extraction rate of H_3PO_4. R_0=6, Stirring rate=300 rpm (linear velocity= 0.785 m/s), φ_{TBP}=80%, T=80 °C, centrifugal speed=4,000 rpm (5,205.4 g), centrifugal time=10 min, and extraction time= 30 min.

CONCLUSION

A new process for separating H_3PO_4 from WSPA by TBP was demonstrated to be feasible. The extraction equilibrium experiments showed that TBP could achieve a single-stage extraction rate of 70% for H_3PO_4. In addition, the H_3PO_4 selectivity is reduced under high H_3PO_4 loading and low-temperature extraction conditions. Under the appropriate extraction conditions, the extraction rates of H_3PO_4, Fe, Al, Mg, and Ca from the WSPA were 69.7%, 7.38%, 6.64%, 4.02%, and 11.8%, respectively. The results of cross-current multi-stage extraction showed that the maximum yield of H_3PO_4, 82.4%, was achieved in two stages. Moreover, in the FT-IR analysis, the peak positions of P=O, P=O···H_2O, and P=O···H_3PO_4 were identified as 1,233, 1,267, and 1,283 cm^{-1}, respectively. By semi-quantitative analysis, the P=O···H_3PO_4 bond was more stable, indicating that P=O tended to bind with the H_3PO_4 molecules in this system compared to H_2O. By analyzing the relationship between $I_{P=O...H_3PO_4}$ and the molar ratio of H_3PO_4 to TBP (k), the CMC value of TBP·H_3PO_4 and two stages of RMs growth were obtained, which corroborated the formation of the third phase resulted from the mutual attraction of the RMs polar cores. In the Raman analysis, a redshift of $\nu_s(P(OH)_3)$ was found in the organic phase, resulting from hydrogen bonding between H_3PO_4 molecules in the RMs. In the scrubbing experiments, the metal ions were removed from the loaded organic phase with a removal rate of 78.47%, 48.53%, 93.56%, and 90.29% for Fe, Al, Mg, and Ca, respectively (R_0=10). In the stripping experiments, it was demonstrated by the McCabe-Thiele analysis that H_3PO_4 could be removed entirely from the organic phase by three stages counter-current at R_0=3.2, T=80 °C, Y_0=0, and X_r=0.02. Finally, the cyclic extraction experiments showed that the extractant had good cycling ability, with the extraction rate

remaining near 70% after ten cycles.

ACKNOWLEDGEMENT

This work was financially supported by National Key R&D Program of China (2016YFD0200404).

NOMENCLATURE AND UNITS

A : peak area
C_i : concentration of component *i* [mol/L]
C : constant
D : distribution ratio
E_i : extraction rate of component *i*
FWHH : full width of half height
g : gravitational acceleration [9.80 m/s^2]
ΔH : molar enthalpy of reaction [kJ/mol]
h : heavy phase
k : mole ratio of H_3PO_4 to TBP
l : light phase
LRP : H_3PO_4 loading ratio of TBP
m : mass [kg]
M : moles per litre
[*i*] concentration of component I [mol/L]
n : mole number
q(i) : mass flow rate of component I [kg/s]
R : universal gas constant [J/(mol·K)]
R : volumetric phase ratio of organic phase to inorganic phase [V^{org}/V^{ino}]
R_0 : initial volumetric phase ratio of organic phase to inorganic phase before extraction or stripping [V^{org}/V^{ino}]
R_e : volumetric phase ratio V^{org}/V^{ino} at extraction equilibrium
Re : removal rate
T : temperature [°C]
V : volume [m^3]
w(i) : mass fraction of component *i*
X_c : peak position
X_n : the mass ratio of H_3PO_4 to TBP in organic phase at the nth stage
X_f : the mass ratio of H_3PO_4 to TBP in feed loading organic phase
Y_0 : the mass ratio of H_3PO_4 to H_2O in feed aqueous phase
Y_{n+1} : the mass ratio of H_3PO_4 to H_2O in aqueous phase at the stage (n+1)

Greek Symbols

$\beta_{i/j}$: separation factor of component *i* towards component *j*
γ : out-of-plane bending vibration
δ : scissoring vibration
ρ : rocking vibration
φ_i : volume fraction of component *i*
ν : stretching vibration

Superscripts & Subscripts

aq : aqueous solution
as : asymmetrical vibration
f : feed state
tl : total liquid collected at the end by stripping
ino : inorganic phase
org : organic phase
r : raffinate phase
s : symmetrical vibration

SUPPORTING INFORMATION

Additional information as noted in the text. This information is available via the Internet at http://www.springer.com/chemistry/journal/11814.

REFERENCES

1. Z. Chen, Y. Ding, B. Long, F. Deng, P. Liu, G. Xiao and Q. Zhang, *Chem. Bioeng.* (Wuhan, China), **32**, 63 (2015).
2. S. Meles and M. V. Prostenik, *Polyhedron*, **3**, 615 (1984).
3. Y. Jin, Y. J. Ma, Y. L. Weng, X. H. Jia and J. Li, *J. Ind. Eng. Chem.*, **20**, 3446 (2014).
4. M. I. El-Khaiary, *Sep. Purif. Technol.*, **12**, 13 (1997).
5. J. Yu and D. J. Liu, *Chem. Eng. Res. Des.*, **88**, 712 (2010).
6. M. Hmamou, B. Ammary, A. Bellaouchou and A. El hammadi, *Mater. Today Proc.*, **24**, 1 (2020).
7. G. Li, Hubei Xingfa Chemical Industry Group Co., T. C. I. R Institute, Phosphoric acid for industry use, GB/T 2091-2008, China National Standardization Administration Committee.
8. M. I. Amin, M. M. Ali, H. M. Kamal, A. M. Youssef and M. A. Akl, *Hydrometallurgy*, **105**, 115 (2010).
9. M. C. Assuncao, G. Cote, M. Andre, H. Halleux and A. Chagnes, *RSC Adv.*, **7**, 6922 (2017).
10. M. Feki, *Chem. Eng. J.*, **88**, 71 (2002).
11. S. J. Zhang, Y. X. Chen, T. Zhang, L. Lv, D. Y. Zheng, B. H. Zhong and S. W. Tang, *Sep. Purif. Technol.*, **249**, 117 (2020).
12. H. Chen, Z. Sun, X. Song and J. Yu, *J. Chem. Eng. Data*, **61**, 438 (2015).
13. M. Chen, J. Li, Y. Jin, J. H. Luo, X. H. Zhu and D. F. Yu, *J. Chem. Technol. Biot.*, **93**, 467 (2018).
14. D. Liu, S. Jiang, H. Luo and Y. Zhang, *Phosphate Compd. Fert*, **20**, 6 (2005).
15. L. Yang, C. Tang, Z. Y. Zhang and X. L. Wang, Chinese Patent, CN106145075A (2016).
16. J. X. Yang, X. J. Kong, D. H. Xu, W. J. Xie and X. L. Wang, *Chem. Eng. J.*, **359**, 1453 (2019).
17. K. E. Mcgill and O. S. Kerns, *Nutr. Cycl. Agroecosyst.*, **25**, 179 (1990).
18. C. E. Breed, K. E. Mcgill and M. T. Holt, *J. Environ. Sci. Health A Tox. Hazard. Subst. Environ. Eng.*, **21**, 609 (1986).
19. M. Y. Huang, K. Yang, J. Li and B. H. Zhong, *Phosphate. Compd. Fert.*, **19**, 9 (2004).
20. B. H. Zhong, J. Li and L. Chen, *Hsien Tai Hua Kung*, **25**, 48 (2005).
21. Y. Jin, D. Zou, S. Wu, Y. Cao and J. Li, *Ind. Eng. Chem. Res.*, **54**, 108 (2014).
22. C. Wei, B. Hu, Y. Li, S. Wang, H. Wuf and J. Pu, *Phosphate. Compd. Fert.*, **33**, 28 (2018).
23. Z. Luo, B. Zeng, K. Luo and B. Wang, *Ind. Miner. Process.*, **43**, 60 (2014).
24. L. Yang, *Phosphate. Compd. Fert.*, **35**, 19 (2020).

25. R. Dhouib-Sahnoun, M. Fekif and H. F. Ayedi, *J. Chem. Eng. Data*, **47**, 861 (2002).
26. Y. Jin, J. Li, J. Luo, D. S. Zheng and L. Liu, *J. Chem. Eng. Data*, **55**, 3196 (2010).
27. C. Liu, J. Cao, W. Shen, Y. Ren, W. Mu and X. Ding, *Fluid Phase Equilib.*, **408**, 190 (2016).
28. K. Ziat, B. Mesnaoui, T. Bounahmidi, R. Boussen, M. Guardia and S. Garrigues, *Fluid Phase Equilib.*, **201**, 259 (2002).
29. C. Q. Liu, Y. Ren and Y. N. Wang, *J. Chem. Eng. Data*, **59**, 70 (2013).
30. Y. Ren, C. Q. Liu, J. Cao, W. Mu and X. Ding, *J. Chem. Eng. Data*, **61**, 1735 (2016).
31. K. Ziat, B. Messnaoui, T. Bounahmidi and M. Guardia, *Fluid Phase Equilib.*, **224**, 39 (2004).
32. D. S. Zheng, J. Li, K. Zhou, J. H. Luof and Y. Jin, *J. Chem. Eng. Data*, **55**, 58 (2010).
33. S. Kouzbour, B. Gourich, F. Gros, C. Vial, F. Allam and Y. Stiriba, *Hydrometallurgy*, **188**, 222 (2019).
34. F. Xun, Z. Yan and H. S. Zheng, *Solvent. Extr. Ion. Exch.*, **20**, 241 (2002).
35. P. H. Tedesco and V. B. Rumi, *Polyhedron*, **42**, 1033 (1980).
36. C. E. Higgins and W. H. Baldwin, *Polyhedron*, **24**, 415 (1962).
37. S. Nave, C. Mandin, L. Martinet, L. Berthon, F. Testard, C. Madic and T. Zemb, *ACS Phys. Chem. Au.*, **6**, 799 (2004).
38. X. T. Yi, G. S. Huo and W. Tang, *Hydrometallurgy*, **192**, 105265 (2020).
39. X. K. Zhou, Z. F. Zhang, S. T. Kuang, Y. L. Li, Y. Q. Ma, Y. H. Li and W. P. Liao, *Hydrometallurgy*, **185**, 76 (2019).
40. R. K. Mishra, P. C. Rout, K. Sarangi and K. C. Nathsarma, *Hydrometallurgy*, **104**, 298 (2010).
41. L. Cui, L. Wang, M. Feng, L. Fang, Y. Guo and F. Cheng, *Green Energy Environ.*, **6**, 607 (2020).
42. Y. Zhao, C. Xing, C. Shao, G. Chen, S. Sun, G. Chen, L. Zhang, J. Pei, P. Qiu and S. Guo, *Fuel* (Lond), **278**, 118229 (2020).
43. W. W. Rudolph, *Dalton Trans*, **39**, 9642 (2010).